Received: 6 February 2021 | Revised: 23 February 2021 | Accepted: 28 February 2021

DOI: 10.1002/jmr.2897

RESEARCH ARTICLE

Journal of Molecular Recognition WILEY

Chemical binding of molecular-imprinted polymer to biotinilated antibody: Utilization of molecular imprinting polymer as intelligent synthetic biomaterials toward recognition of carcinoma embryonic antigen in human plasma sample

Parinaz Abdollahiyan[1] | Arezoo Mohammadzadeh[2] | Mohammad Hasanzadeh[1]

[1]Pharmaceutical Analysis Research Center, Tabriz University of Medical Sciences, Tabriz, Iran

[2]Food and Drug Safety Research Center, Tabriz University of Medical Sciences, Tabriz, Iran

Correspondence
Mohammad Hasanzadeh, Pharmaceutical Analysis Research Center, Tabriz University of Medical Sciences, Tabriz, Iran.
Email: hasanzadehm@tbzmed.ac.ir

Abstract

In this study, a novel biosensor based on molecular imprinting polymer (MIP) methodology was fabricated toward recognition of carcinoembryonic antigen (CEA). For this purpose, poly (toluidine blue) (PTB) was electropolymerized on the surface of gold electrode in the absence and presence of CEA. So, the target molecules were entrapped into the imprinted specific cavities of MIP. Obtained results show that, the binding affinity of the MIP system was significantly higher than that of revealed for the nonimprinted polymer (NIP) system, MIP-based biosensor revealed linear response from (0.005 to 75 μg/L) and low limit of quantification of (0.005 μg/L) by using chronoamperometry technique, leading to CEA monitoring in real and clinical samples. Thus, a novel technique for rapid, simple, sensitive and affordable monitoring of CEA (LLOQ = 0.005 μg/L) has provided through developed biosensor. From a future perspective, moreover, this method can be considered as an applicable candidate in biomedical and clinical analysis for point-of-care usages.

KEYWORDS
biomedical analysis, carcinoembryonic antigen, chemical binding, electropolymerization, molecular imprinting

1 | INTRODUCTION

With the aim of raising the efficient cancer therapy, early diagnosis of cancer disease is considered as one of the most challenging issues today. Detection of cancer biomarker leads to provide the opportunity of diagnosis the disease, before it grows into the incurable stages.[1-3] Furthermore, biomarkers can be applied to assess the progression of surgery treatments. Carcinoembryonic antigen (CEA), one of the most common cancer biomarkers, is a glycoprotein in human body that is expressed during the fetal development.[4] This biomarker, which can be found in adult human plasma sample (HPS) in slight amounts, will represent overexpressed behavior in several cancers, including pancreatic, ovarian, breast, gastric, lung cancers, and in particular, colorectal cancer.[4] Therefore, CEA detection has gained great interest in therapeutic evaluation, condition monitoring, and differential diagnosis of diseases.[4]

The conventional CEA measuring methods are typically based on immunoassay tests. However, these immunoassay tests require expensive and complex instruments and expert operators.[5] Besides, there is the risk of hazardous radioactive elements that may cause to harmful effects on the patients' body.[6] Regarding improving tumor biomarkers detection, novel bio-affinity sensors have widely studied and have satisfactorily used for addressing all the aforementioned issues and have considered as efficient analytical tools.[7] Biomolecular receptors (eg, histones, enzymes, and antibodies) are being replaced with non-natural diagnostic elements; in particular, MIPs are

intelligent synthetic biomaterials that can imitate biological recognition; thus, the MIPs materials are called as "plastic antibodies".[8]

Recently, MIP-based bio-devices have been increasingly considered as promising analytical tools in various fields, comprising clinical analysis, providing required portability, low cost, specificity, and fast response.[9] This method was first described, at 1930s, as "the fabrication of ligand-selective diagnostic sites throughout a synthetic polymer film where a specific template (ion, molecule, atom complex or a macromolecular ionic, or molecular assembly) is applied with the purpose of promoting formation of the recognition site during a polycondensation or polymerization process, following by the elimination of all or some of the specific templates required for diagnosis to remain the cavity spaces..[10-12] In comparison with the other diagnostic techniques, MIPs, which comprise three main unique characters of application universality, recognition specificity, and structure predictability, have found broad interest and have become useful in several areas, such as separation and purification,[13] bio/chemosensing,[14] drug delivery,[15] artificial antibodies,[16] and catalysis,[17] respect to their straightforward preparation, high physical stability, affordability, and remarkable robustness.[18] Bulk polymerization is a conventional method for molecular imprinting.

Recently, several systems have emerged that apply a variety of techniques to fabricate imprinted particles that have better structures than that of the conventional methods.[19] Chief among the other strategies, electropolymerization techniques are known as efficient methods for MIPs deposition on various types of electrodes.[20] The superiority of electropolymerization methods among others is based on their potential to deposit the polymeric films on irregularly shaped or tiny dimension electrode surfaces, with adjustable thickness.[21] The thickness of the deposited conducting and nonconducting films can be controlled upon the rate of charge transfer and self-regulation, respectively.[22,23] Furthermore, the type of the film and the polymerization rate can be regulated via the potential applied during electropolymerization.[24,25]

In this work, poly [Toluidine Blue (PTB)], an electrically semiconducting polymer, was considered as the artificial receptor, modified by molecular imprinting techniques and organized by electrochemical approach for the sensitive monitoring of CEA. With this regard, gold electrode, which has been pretreated by cysteamine and glutaraldehyde (Cys A-GA), was applied as the substrate where the protein-imprinted polymer was electropolymerized. The stability of the synthesized MIP system against degradation was considerably boosted, owing to the crosslinking role of the Cys A-GA modifiers that led to firm covalent bonds between the polymer film and the gold surface. The ability of the synthesized MIP bioreceptor toward CEA recognition was evaluated by electrochemical techniques. The binding affinity of the nonimprinted polymer system (NIP) was significantly lower than that of MIP system, confirming the accomplishment of the technique in creating imprinted materials to CEA recognition. In addition, the redox peak current of the $Fe(CN)_6^{3-/4-}$ showed an ascending trend by raising the concentration of CEA (from 0.005 to 60 μg/L) incubated with the MIP-coated electrode. The biosensor revealed linear response by increasing the concentration from 0.005 to 75 μg/L and also LLOQ of 0.005 μg/L by means of chronoamperometry technique, leading to sensitive and selective monitoring of the CEA in real samples. The suggested MIP-based biodevice was considered for assessing of CEA amounts in human plasma serum. The developed biosensor offers a novel diagnostic method, for the first time, toward rapid, simple, sensitive, and cost-effective recognition of CEA through MIP methodology. The proposed technique can also be appeared as an efficient candidate for POC usages in biomedical and clinical analysis.

2 | MATERIALS AND METHODS

2.1 | Chemical and reagents

Toluidine blue (C.I. 52 040) with purity of 99% was purchased from Merck pharmaceutical company (Germany). KCl, potassium ferricyanide $K_3Fe(CN)_6$, and potassium ferrocyanide $K_4Fe(CN)_6$ were obtained from Sigma-Aldrich chemicals company (Ontario, Canada). Hydrochloric acid, human serum albumin (HSA), and (HCL)HNO_3 were also bought from Scharlau Chemie S.A. The solution of phosphate buffer saline (PBS) (0.1 M, pH = 7.4) was obtained by NaH_2PO_4 (0.1 M), and Na_2HPO_4 (0.1 M) in deionized (DI) water. The human plasma samples were purchased from the Iranian Blood Transfusion Research Center (Tabriz, Iran). CEA, biotinylated antibody, dilute solutions, Human Cancer Antigen PSA ELISA Kit containing PSA antigen, Human CA 15-3 ELISA kit (CanAg/CA15-3 EIA) containing CA 15-3 antigen, and standard buffer were purchased from CanAg Diagnostic AB Technology Co. (Gothenburg, Sweden), Human CEA ELISA kit (CanAg/CA15-3 EIA) containing CEA antigen, and standard buffer were purchased from CanAg Diagnostic AB Technology Co. (Gothenburg, Sweden).

2.2 | Apparatus

Electrochemical analyses were performed by a computer-guided electrochemical system including AUTOLAB device with PGSTAT302N (Eco Chemie, Utrecht, The Netherlands), by means of NOVA 1.11 software. The conventional system of three-electrode electrochemical cell was applied by a platinum wire, Ag/AgCl, and gold electrode as the counter, reference, and working electrodes, respectively. Electrochemical characterization of the MIP-based biosensor was performed by CV method in the presence of $Fe(CN)_6^{3-}/Fe(CN)_6^{4-}$ (1 mM) containing KCL (0.1 M) through a potential range from −0.5 to 0.7 V (vs Ag/AgCl), at a scan rate about 40 $mV{\cdot}s^{-1}$. The morphology of the modified electrode surface was monitored by a high-resolution field emission scanning electron microscope (FE-SEM, Hitachi-SU8020, Czech) system, with an operating voltage about 3 kV. Chemical compounds were evaluated using energy dispersive spectroscopy (EDS).

2.3 | TB electropolymerization on the surface of the pretreated gold electrode

First, the surface of the electrode was cleaned by H_2SO_4 solution (0.1 M) through cyclic voltammetry technique with the potential range

of 0 to 1.5 V and at scan rate of 100 mV/s over 15 cycles. Then, cysteamine solution (10 mM) was casted on the surface of gold electrode for 1 hour. Afterward, the Au electrode was further treated with glutaraldehyde as cross-linker for another 1 hour. Next, the gold electrode was polymerized though electropolymerization approach by applying TBs in PBS solution (pH = 7.4) through CV technique within the potential range of −0.5 to 0.7 V and at scan rate of 40 mV/s over 60 cycles (Figure 1). Finally, the gold electrode was further treated (1 M) KNO_3 in PBS solution (pH = 7.4) using CV method within the potential range of −0.3 to 0.5 V and at the scan rate of 40 mV/s over 10 cycles.

The surface-related factors, such as the rate of the applied template/monomer, dens of polymer film, and etc., were adjusted regarding to improve the analytical performance of the proposed MIP-based biodevice for the sensitive and selective monitoring of CEA in both of the standard and HPS samples. Concerning the efficient surface imprinting, the dense of the PTB coating should be in proportion with the symmetrical dimension of anchored protein biotemplates. Hence, due to the high MW (≈180 kDa) and large dimensions of CEA, the electroconductive polymer veneer was grown until appearing the extreme electrocatalytic behavior.

In this work, the surface of the working gold electrode was cleaned through CV technique, in the presence of H_2SO_4 solution (0.1 M) with the potential range of 0 to 1.5 V, scan rate of 100 mV/s, and over 15 cycles. Afterward, the electrode was functionalized via amine and aldehyde groups by incubating in cysteamine solution (10 mM) and glutaraldehyde (5%), for 1 hour, respectively. At the next step, the premodified gold electrode was polymerized by applying TBs (0.1 M) in PBS solution (pH = 7.4) (0.1 M), in the presence of CEA antigen through CV method with the potential range of −0.5 to 0.7 V, scan rate of 40 mV/s, and over 60 cycles. Afterward, the PTB-coated gold electrode was treated by means of KNO_3 (1 M) in PBS solution (pH = 7.4) via CV method with the potential range of −0.3 to 0.5 V, scan rate of 40 mV/s, and over 10 cycles. Finally, the surface of the prepared electrode was eluted via 0.1 M NaOH solution through CV method with the potential range of −0.3 to 0.5 V, scan rate of 50 mV/s, and over 100 cycles.

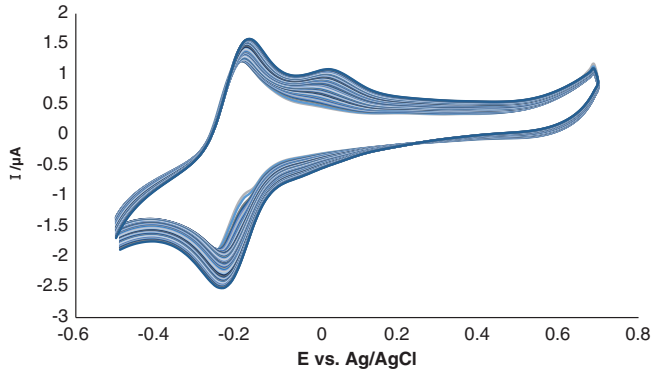

FIGURE 1 Cyclic voltammogram of electropolymerization of TB on the surface of the gold electrode in the presence of 0.5 mM of TB in 0.1 M PBS (pH 7.4) at 40 mV/s^{-1} with 60 number of cycles

As schemed in Scheme 1, the cleaned surface of the working electrode is pretreated with the cross-linkers, using cysteamine and glutaraldehyde, respectively. Then, the modified surface is covered by PTB film in the presence of CEA as bio-templates. The CEA molecules are entrapped within the polymer matrix through covalent interactions between the amine groups of the PTBs and the carboxylic acid groups of the CEA biomarkers. TB is a tiny redox-active phenazine material that supply a positive charge with N replaced by S in the azine ring and amine or methyl functional groups of the benzene rings. Numerous H-bonds and electrostatic interaction between the N-H/O-H groups of CEA biomarker, and the S-H/N-H groups of TB might be the chief cause for the formation of the polymer-protein layer. Finally, the prepared biosensor is washed via 0.1 M NaOH solution for elimination of the protein bio-template and MIP preparation. In comparison with the PTB film, the results revealed the inhibitory effects of the CEA biotemplates on the growth of the PTB film, after entrapping within the polymer matrix.

3 | RESULTS AND DISCUSSION

3.1 | Electropolymerization of TB on the surface of gold electrode

As mentioned before, the gold electrode was premodified with GA-Cys A. The complex of the cross-linker is constructed through covalent bindings between the amine groups of Cys A with the aldehyde groups of GA. On the other side, the complex of cross-linkers can make firm binds with the surface of the gold electrode via thiol groups. According to Figure 1, CV method was applied to form PTB on the premodified electrode, in potential range from −0.5 to 0.7 V vs Ag/AgCl, and scan rate of 40 mV/s, through 60 cycles. During the electropolymerization process of TB, anodic peaks and reduction peaks started to be appeared at −0.1 and − 0.2 V vs Ag/AgCl, respectively, which confirm the formation of PTB on the gold electrode. Also, increase in the current intensity of the peaks by raising the cycle numbers showed the growth of the PTB on the gold surface. Finally, Figure 1 revealed the dwindling of the oxidation peak after formation of the PTB film. It has been affirmed that TB monomers, who contain amine groups (-NH_2) in their chemical structures, can be electropolymerized on the gold surface to create a conducting film through covalent bonds between the NH_2 groups of TB and the aldehyde groups of GA with considerable stability. Regarding to confirm the PTB formation on the gold surface, CV was performed through the redox probe $([Fe(CN)_6]^{3-/4}$, in the potential range of −0.3 to 0.5 V vs Ag/AgCl, at 100 mV/s.

FE-SEM analysis was done to detect the morphology of PTBs/Au, PSA/PTBs/Au, and MIP/PTBs/Au electrodes. As shown in Figure S1 (see supporting information), the polymerization of TB leads to construction of a dendrite morphology on the surface of Au electrode, which provides highly dense PTBs for subsequent imprinting of the target molecule. The weight percentages of elements, including

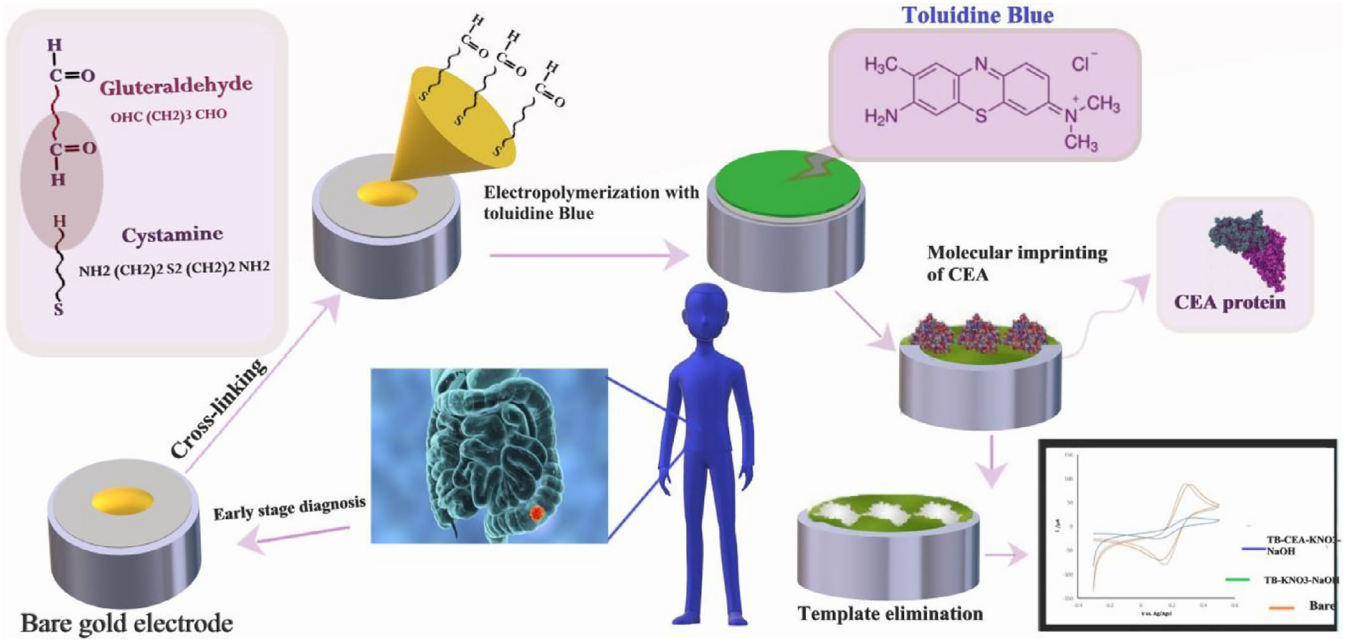

SCHEME 1 The step-by-step procedure of cancer diagnosis in the early stages, based on sensitive CEA detection via MIP-based immunosensor, taking advantage of electroanalytical approaches. CEA, carcinoembryonic antigen

carbon, nitrogen, and oxygen were obtained 4.77, 2.26, and 92.97, respectively, by the EDX spectrum. The results showed that the considerable weight percentages of carbon, nitrogen, and oxygen were obtained as a result of the PTBs formed on the surface of gold electrode. Also, Figure S2 (see supporting information) shows FESEM images of MIP and NIP which confirmed successful preparation of biosensor platform.

3.2 | Electrochemical characterization

The in-depth electrochemical behavior of the stepwise fabrication process of the designed biosensor (MIP-PTB and NIP-PTB films coated on gold electrode) was evaluated through CV and chronoamperometry techniques in 0.01 M $[Fe(CN)_6]^{3-/4-}$ as illustrated in Figure 2, and Table 1. Figure 2A reveals redox peaks of the bare gold electrode (red line). The oxidation peak of the bare gold electrode was appeared at 0.2 V vs Ag/AgCl with current intensity about 33.67 μA, which was slightly decreased to 27.11 μA after treating with CysA. The reason of this slight reduction in the electric current can be attributed to the increment in the geometric surface area in the presence of Cys-A. Moreover, the presence of an electrically hindrance layer of CysA on the highly conductive gold electrode, which leads to raising the electrical resistance, and consequently, diminishing the electron transfer process. The negligible decrement in the redox peak of the Cys A-modified electrode can also be related to the presence of the free unbonded amine groups on the surface of the gold electrode after CysA modification. Therefore, the electric current intensity of the redox peak was raised to 38.67 μA after modifying with GA, due to the increment in the stability of the system by making covalent binds between the amine groups of the CysA, and the aldehyde groups of GA. Considering the bare electrode as the control sample, the oxidation peak had slight increment after electro-polymerization of TB (Figure S3). The increment of the anodic current reveals that the conductive PTB layer can promote electron transfer of 0.01 M $[Fe(CN)6]^{3-/4-}$. When the CEA bio-templates were interacted with the polymer matrix through hydrogen bonds between the amine groups of the PTBs and the carboxylic acid groups of the proteins, the response current of the MIP-modified electrode was considerably decreased which indicates the immobilization of CEA is carried up properly and retracted electron transfer (Figure S4). In fact, the protein templates assume the role as an insulter and dwindle the rate of the electrons motion. After template elimination from the polymer matrix, the relevant cavities of the entrapped CEA molecules were appeared. The redox peak currents of the MIP-based PTB coated gold electrode were dramatically increased again in comparison with that of CEA/PTB/gold electrode (from 0 μA (for TB-treated electrode) to 17.5 μA (0.2 V vs Ag/AgCl) (for CEA eliminated PTB coated electrode)) (Figure 4, and Figure 3), due to the repulsive interactions of the negatively charged MIP polymer with the supporting electrolyte. Additionally, the presence or absence of the template protein causes to structural differences for the electropolymerized films, which can be detected through the redox probe ($[Fe(CN)_6]^{3-/4}$) alternations. All of abovementioned results were summarized in Table S1.

Thus, the entrapment of the bio-template within the polymer veneer can be confirmed through the hindrance behavior of the electrochemical surface blocking redox procedure of Fe (III)/Fe (IV). It is noteworthy, moreover, that the hindrance behavior of MIP is more

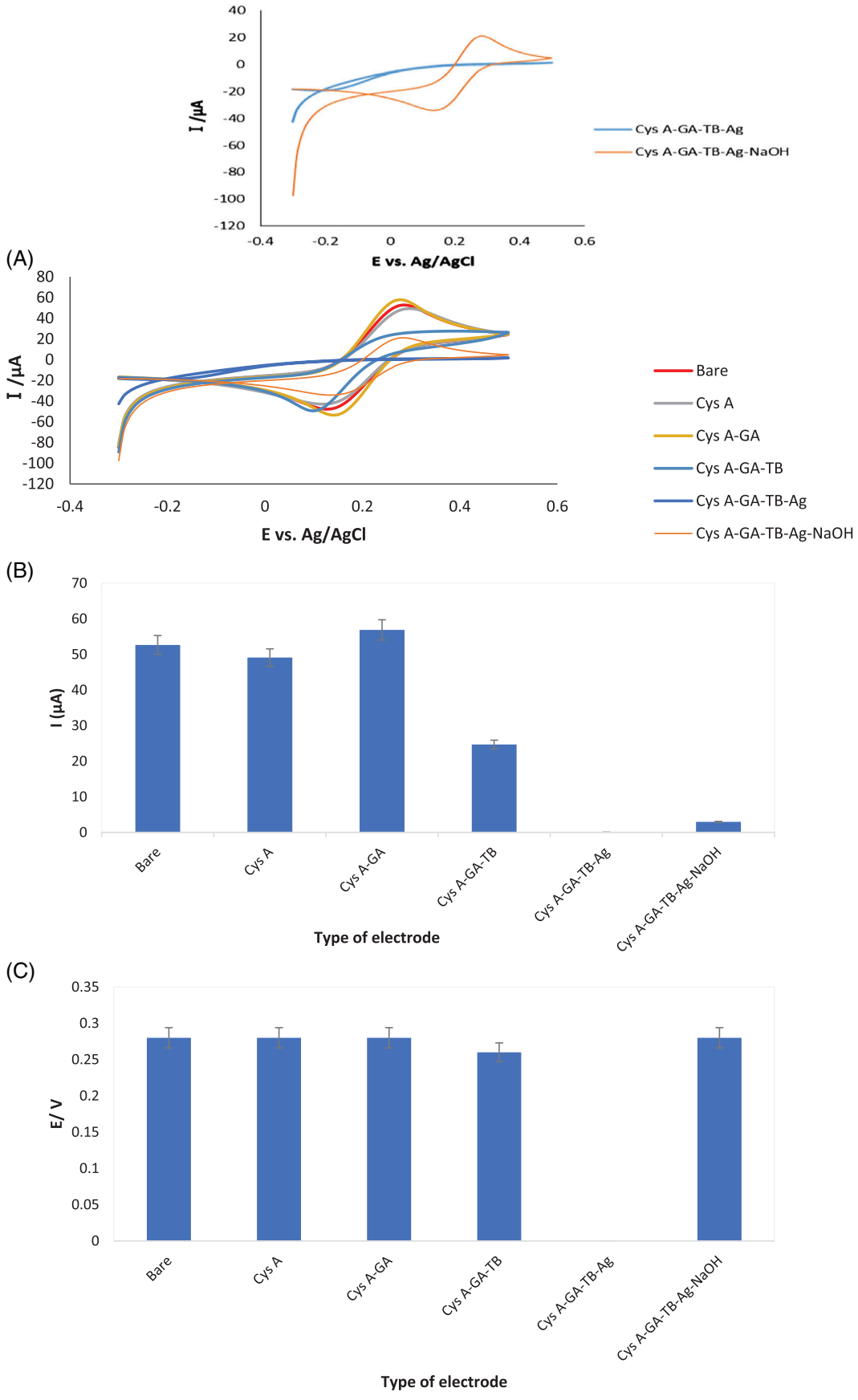

FIGURE 2 A, CVs of Au, Au-Cys A, Au-Cys A-GA, Au-Cys A-GA-p(TB), Au-Cys A-GA-p(TB) + CEA, and MIP in the presence of 0.1 M $[Fe(CN)_6]^{3-/4-}$ containing KCl, in the potential range of −0.3 to 0.5 V, scan rate of 0.1 V/s. B, C. Histogram of peak current and potential vs type of electrode, respectively. (n = 3, SD = 1.74)

TABLE 1 The comparison of various immunosensors for CEA detection

Detection technique	Applied materials	Detection range	LOD	Ref.
Electrochemical (DPV)	Zwitterionic poly(carboxybetaine) functionalized polyaniline nanowires	1.0×10^{-14} g.mL^{-1} to 1.0×10^{-10} g.mL^{-1}	3.05 fg mL^{-1}	[26]
Electrochemical (DPV) and (EIS)	Ag/MoS_2@Fe_3O_4	0.0001-20 ng mL^{-1}	0.03 pg mL^{-1}	[27]
Electrochemical (DPV)	Cu_2O-Carbon Dot, and gold nanoparticle	1.0 pg mL^{-1} to 0.001 g mL^{-1}	0.19 pg mL^{-1}	[28]
Electrochemical (DPV)	Prussian Blue, carbon nanotube, and graphene	0.2-1.0, and 1.0-40.0 ng·mL^{-1}	60 pg·mL^{-1}	[29]
Electrochemical (DPV)	Isatin-based immunosensor	50.0 pg mL^{-1}-100.0 ng mL^{-1}	0.29 ng mL^{-1}	[30]
Amperometric	Graphene-nafion nanocomposite film	0.5 to 120 ng mL^{-1}	0.17 ng mL^{-1}	[31]
Amperometric	Molybdenum (Mo), bismuth oxide (Bi_2O_3)	1 pg mL^{-1} to 1 μg/mL	0.3 pg mL^{-1}	[32]
Fluorescence	Aptamer hairpin	10 pg mL^{-1} to 500 ng mL^{-1}	4.2 pg mL^{-1}	[33]
Fluorescence	Molybdenum disulfide nanosheets	100 pg mL^{-1}-100 ng mL^{-1}	34 pg mL^{-1}	[34]
Fluorescence	Thioflavin T, AgNCs	0.5-20 ng mL^{-1}	0.1 ng mL^{-1}	[35]
Electrochemical (SWV)	poly(ferrocenyl glycidyl ether)-grafted CNTs (PFcGE-CNTs)	1×10^{-15}-1 $\times 10^{-8}$ g.mL^{-1}	2.8×10^{-16} g mL^{-1}	[36]
Electrochemical (CV) and (chronoamperometry)	MIP-based poly toluidine blue treated gold electrode	0.005 to 75 μg/L	0.005 μg/L	This work

operative than that of NIP, due to the combination of both earlier effects in this process.

In this project, the optimized washing condition was considered in 0.1 M NaOH for CEA elimination through the potential cycling process of the Au electrode over100 cycles at 0.1 V/s, between −0.3 to 0.5 V; followed by washing with DI water. The significant raise of the current intensity after elution, indicated successful elimination of the CEA biotemplate, which acted as a barrier for the electric current. Additionally, according to Figure 2C, for optimal recognition of CEA, the protein elimination process needs the constant potential of +0.29 V, which is considerably lower than that of before elution (+0.49 V). Lower potential reveals less interference by the electrochemically active materials in the biological media. This is affirmed by interference studies in presence of other biomarkers, as interferers (Figure 3).

The chief operation of a sensor is its potential of recognition the specific molecular targets among other interfering agents. Therefore, the selectivity of the designed bio-device was evaluated in the presence of PSA, BSA, CA 15.3 and HSA as interfering species. According to Figure 3, The peak intensity of MIP/CEA/PTB/gold electrode was measured by chronoamperometry, and CV techniques in Fe $(CN)_6^{3-/4-}$ comprising KCl (0.1 M) solutions with the potential range about −0.3 to 0.5 V. Figure 3A, B reveals the CVs and their relevant histograms of electric current intensities of the MIP-based gold electrodes in the presence of various biomarkers (as interferences). It is obvious that the electric current intensity of the MIP-treated electrode is dramatically lower in the presence of CEA (21.02 μA) than that of the other proteins (78.61 μA, 69.22 μA, 62.2 μA, and 63.7 μA, for HAS, PSA, CA 15.3, and BSA, respectively). Besides, the chronoamperograms and their relevant current intensity histograms (in Figure 5C,D) confirm the aforementioned decrement in the electric current intensity of the MIP-treated Au electrodes in the presence of CEA (1.09 μA) vs that of the other interferences (11.51 μA, 9.49 μA, 9.75 μA, and 9.12 μA for HAS, PSA, CA 15.3, and BSA, respectively). This significant increment in the electric current rate of the MIP-treated electrode in the presence of CEA reveals more entrapment of CEA biomarkers in the imprinted cavities of the modified electrode, compared to the other interferences, which acted as insulators for electric current. Thus, the results indicated that the recognition of CEA bio-agent was considerably higher than those for PSA, HAS, BSA, and CA 15.3. As confirmed in Figure 5, evident is the fact that the synthesized protein-imprinted polymer shows an apparent selectivity towards CEA, because of the specific molecular structures of the imprinted sites which accurately resemble the dimensional features of the CEA antibody.

High selectivity to CEA, as the target molecule, is apparently found on the prepared MIP-PTB gold electrode, with a perspective of cancer detection in early stages.

Besides cyclic voltammetry, chronoamperometry was employed for the evaluation of the process occurring via electro-polymerization of TB, as well as the MIP process of the bio-template. Chronoamperograms were recorded at the potential of 0.3 V *vs* Ag/AgCl, through 50s. The chronoamperogram analysis were recorded by adjusting the potential of the working electrode to the desired values that was applied to estimate the rate of catalytic constant on the engineered surface. The sensing features of the proposed immunosensor was evaluated in every single

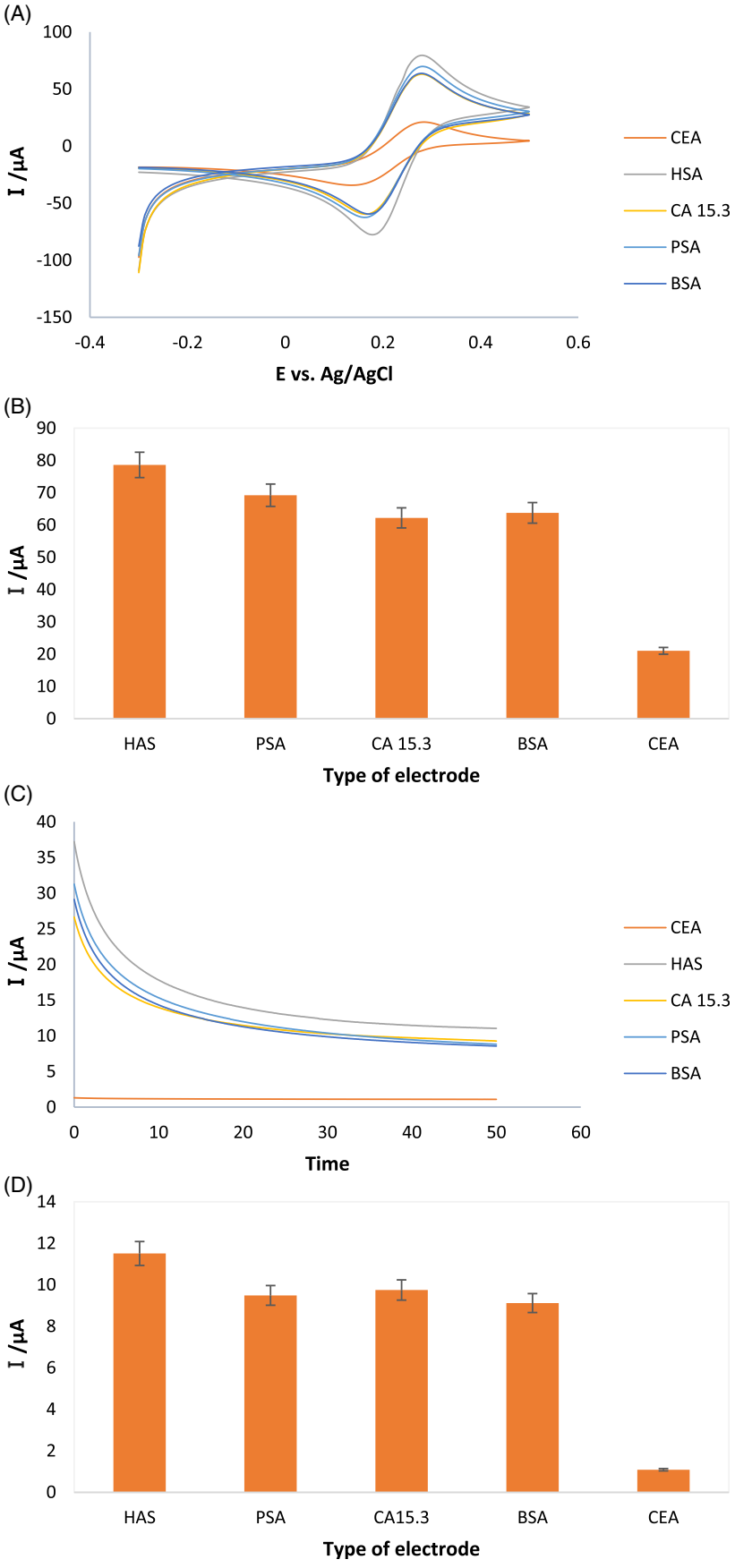

FIGURE 3 CVs and chronoamperogram (E = 0.27 V) CEA/PTBs/gold electrode in the presence of different interferent species (BSA, HAS, PSA, CA 15-3) after removal CEA antigen from the polymeric structure in the solution 0.1 M $[Fe(CN)_6]^{3-/4-}$ containing KCl, respectively, A, C. Histograms of the variations of the current peaks (B, D). (n = 3, SD = 2.22). Parameters: the potential range of −0.3 to 0.5 V with a scan rate = 50 mV/s. CEA concentration is 2 µg/L

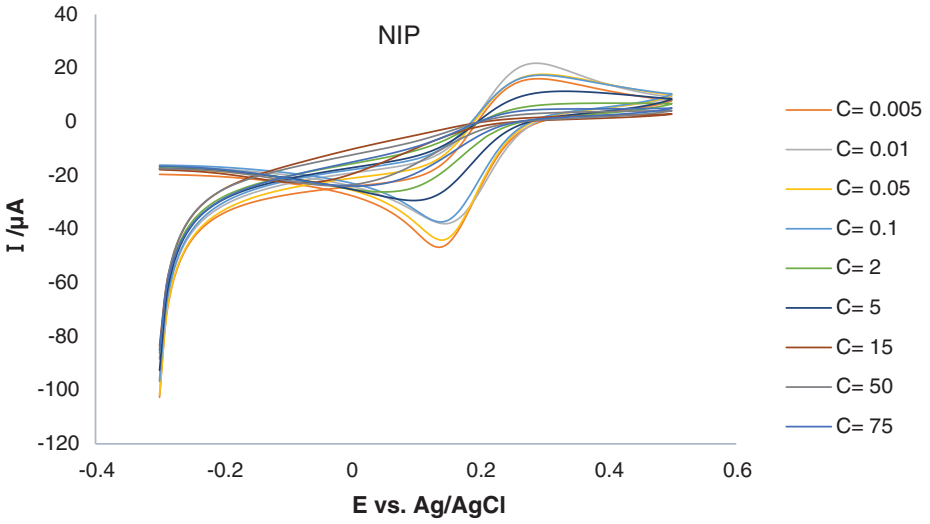

FIGURE 4 The comparative CV diagrams of CEA/PTBs/gold electrode in different concentration of CEA (75, 50, 15, 5, 2, 0.1, 0.01, 0.05, 0.005 µg/mL) before removal CEA antigen from the polymeric structure in the solution 0.1 M $[Fe(CN)_6]^{3-/4-}$ containing KCl. Potential Range = 0.5 to −0.3. Scan Rate: 50 mV/s. Inset is calibration curve

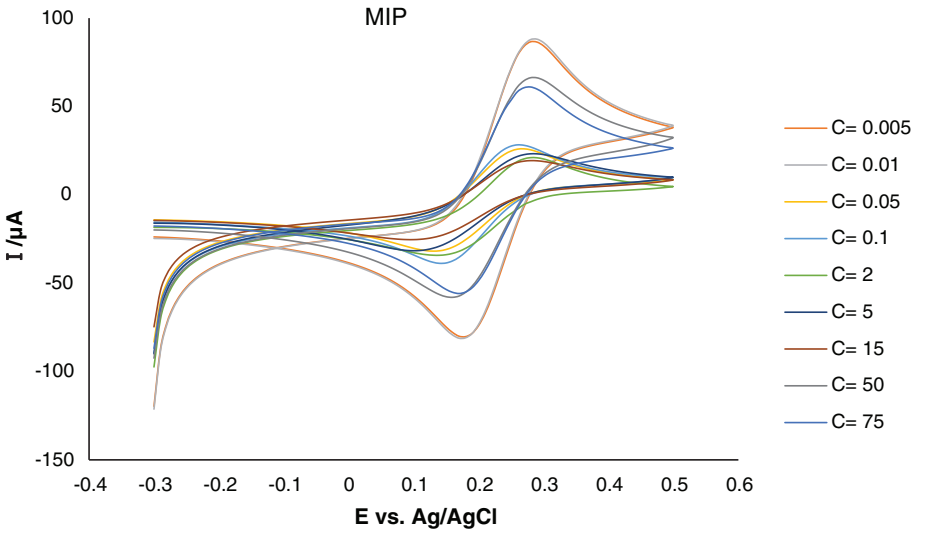

FIGURE 5 The comparative CV diagrams of CEA/PTBs/gold electrode in different concentration of CEA (75, 50, 15, 5, 2, 0.1, 0.01, 0.05, 0.005 µg/mL) after removal CEA antigen from the polymeric structure in the solution 0.1 M $[Fe(CN)_6]^{3-/4-}$ containing KCl. Scan rate: 50 mV/s

steps of the preparation via single-potential step chronoamperometry analysis (Figure S5). In confirmation with the CVs results, Figure S5, reveals the striking reduction of the electric current intensity after CEA incorporation, which further affirms the insulating behavior of the entrapped protein template. Thus, the intensity of the electric current raise to 1.09 µA after bio-template removal. Moreover, in verification with Figure 2, Figure S5 shows the negligible raise in the current intensity of the bare electrode after modification with Cys-A, and GA, revealing the increment in the surface area of the bare electrode after modification with the mentioned cross-linkers.

3.3 | Analytical performance

3.3.1 | Sensitivity study of the designed immunosensor in exposure to different concentrations of CEA biomarker

The analytic features of the engineered immunosensor in this paper was studied by the CV technique in exposure to various concentrations of CEA biomarker to evaluate the potential of the methods to recognize this protein. Figure 3A shows the CV results for various concentrations of CEA protein in a standard sample, the sweep rate was of 40 $mV.s^{-1}$, and the potential range was −0.5 to 0.7 V vs Ag/AgCl through 60 cycles. Besides, the calibration curves of the different concentrations of CEA represent the linear regression equation for various concentrations of CEA biomarker, ranging from 0.005 µg/L to 75 µg/L of the standard sample, which indicated the high sensitivity of the fabricated immunosensor (data are not shown). According to Figure 4, after incubation of various concentrations of CEA (from 0.005 µg/L to 75 µg/L) to the gold surface electrode modified by CysA-GA-PTB, the peak currents were diminished by raising the concentration of CEA biomarker. In fact, insulation of the gold surface by CEA biomarkers decreases the efficiency of the electron transfer from the supporting solution, and decelerates the electron exchanging rate. Thus, the decreasing trend of the electric current by raising the concentration of the biomarker (as shown in Figure 4), indicates the satisfactorily immobilization of CEA on the surface of the modified gold electrode. The obtained results showed that the proposed immunosensor has the potential for successfully detection of

the CEA biomarker with different concentrations ranging from 0.005 μg/L to 75 μg/L.

LLOQ for CEA detection was obtained as 0.005 μg/L. At the next step, the CEA bio-templates were eliminated from the PTB matrix, through an elution procedure. The functionality of the proposed immunosensor is attributed to the unique structures of the cavities that were appeared after the removal of the entrapped CEA. With this regard, the elution process was performed for the modified PTB-coated electrodes with various concentrations of CEA in the presence of NaOH (0.1 M), at the potential range between −0.5 to 0.7 V *vs* Ag/AgCl, scan rate of 50 $\mu A.s^{-1}$, and under 100 cycles through CV technique (Figure 4). Figure 4B reveals the calibration curves of the elimination of different concentrations of CEA; the results represent the linear regression equation for elimination of various concentrations of CEA biomarker from the PTB matrix, ranging from 0.005 μg/L to 75 μg/L of the standard sample, which indicated the high sensitivity of the fabricated immunosensor. According to Figure 4B, after elimination of various concentrations of CEA (from 0.005 μg/L to 75 μg/L) from the polymer matrix, the peak currents were increased by raising the concentration of CEA biomarker. In fact, since the CEA biomarkers on the gold surface has acted as the electron transfer hindrance, the elimination of these bio-templates caused to accelerate the electron exchange through the supporting media. Thus, the electric currents were increased by raising the concentration of the eliminated protein templates, as shown in Figure 4. Figure 5 indicates the satisfactorily removal of CEA from the polymer matrix coated on the modified gold electrode. The obtained results showed that the proposed immunosensor has the potential for successfully detection of the CEA biomarker with different concentrations ranging from 0.005 μg/L to 75 μg/L. Furthermore, in Figure 5, the calibration curves for low concentrations (0.005 μg/L) and high concentrations (75 μg/L) were plotted. The obtained linear regression equations were as follows:

$$I\,(\mu A) = 0.2479[C_{CEA\,(\mu g/L)}] + 42.574, R^2 = 0.0556.$$

LLOQ for CEA detection was obtained as 0.005 μg/L.

It is noted that the fabricated biosensors exhibit higher sensitivity in the presence of lower concentrations of the bio-template (CEA), than that of higher concentrations which reveals that the greater number of electrons are transferred. Moreover, acceptable electron transfer in higher concentrations of CEA (for both MIP- and NIP-based biosensors) indicated that there is no limiting factor in the detection process.

3.3.2 | Real sample analysis

The bio-sensor was occupied for detection of CEA in human plasma samples incorporating different concentrations of CEA (0.005 μg/L to 75 μg/L) using the standard addition technique. To evaluate the practical usages of bio-imprinted polymer, various concentrations of CEA were incorporated with HPS and determined by CVs and chronoamperometry techniques, after and before bio-template (CEA) elimination. CEA monitoring was performed in exposure to the biological-interfering factors to estimate the efficacy of the fabricated MIP-based biosensor. With this regard, various concentrations of CEA antigen were incorporated into the HPS without dilution or pretreatment, and the redox performance of $Fe(CN)_6^{3-/4-}$ was evaluated by CV (Figure S6), and chronoamperometry (Figure S6) upon CEA binding to the engineered surface. The obvious increment in the current peak of the CEA-TB coated electrode after CEA elimination indicated the successful removal of the protein templates, which had acted as insulator through the conducting polymer matrix (Figure S7A). Moreover, the apparent increment in the slop of the calibration curves of the CEA-PTB chronogram after CEA elimination, from −0.0055 to −0.011 confirms the sensitivity of the proposed biosensor towards CEA detection.

As illustrated in Figure S7, the prepared MIP-based biodevice can clearly determine CEA with various concentrations ranging from 0.005 to 75 $\mu g.L^{-1}$, and the relevant calibration curve to the linear regression equation is measured as follows:

$$I\,(\mu A) = -0.0055[C_{CEA\,(\mu g/L)}] + 3.7424, \text{By chronoamperometry before CEA elimination.}$$

$$I\,(\mu A) = -0.011[C_{CEA\,(\mu g/L)}] + 8.6647, \text{By chronoamperometry after CEA elimination.}$$

$$I\,(\mu A) = -0.0164[C_{CEA\,(\mu g/L)}] + 10.44, \text{By CV before CEA elimination.}$$

$$I\,(\mu A) = -0.0347[C_{CEA\,(\mu g/L)}] + 59.61, \text{By CV after CEA elimination.}$$

Additionally, the optimized recognition potential of the imprinted biodevice, besides the electro-catalytically behavior and the biocompatibility of the prepared PTB were measured by estimating the optimal value of LLOQ. The estimated LLOQ in this work was lower than the previously studied techniques, such as flow injection tests, spectrophotometric techniques, and paper-based microfluidic devices (Table 1).

The main advantage of the MIP method is its selective binding ability to the pattern molecule. Other benefits of the MIP-type biomaterials are including[37,38]:

(1) providing 3D network, where the target molecules can be trapped. Afterwards, the trapped molecules can be removed from the polymer substrate through the washing process, which causes to remain the dimensionally similar cavities with the target molecules.

(2) The simple and affordable preparation procedure.

(3) More sensitive and efficient system than the conventional methods.

Chief among all of the MIP preparation methods (eg, spin-coating,[39] composite making,[40] or drop-coating[41]), electrochemical polymerization has found great interest owing to their unique merits such as fast, and simple preparation procedure, making firm binds with

the surface of the electrode, high reproducibility in various conducting materials, and easy control over the morphology and the thickness of the polymer film. Despite their excellent electrochemical behavior and great electropolymerization ability, there are few studies who has employed phenazines for molecular imprinting of proteins.[8] These types of polymers can maintain the redox activity of the monomers; hence, their conducting nature makes them a favorable candidate for electroanalysis studies. Among these polymers, toluidine blue, a water-soluble member of the redox dye group, has unique electrochemical and chemical features that make it attractive as an electronic mediator in enzyme-based biosensors.[42] Although phenazines can be directly electro-polymerized on the surface of the bare electrode, sometimes, the weak binding between the electrode and the growing phase leads to inhibit the nucleation of the monomers on the electrode surface, and thus, an unstable polymer film may be formed.[43] Alternatively, the polymer coating can be formed from the self-assembled well-organized monolayers promoting the binding stability of the film on the electrode. In this study, we use TB monomers to form the electro-conductive MIP-based biosensor, which has not previously reported for CEA detection. In comparison with the conventionally used immunoassays for CEA detection, designed disposable biosensor can be fabricated through a simple and costly affordable procedure, proposing the possibility of CEA monitoring in POC biosensors with admirable selectivity and sensitivity. Additionally, the stability of our designed bio-system has further improved respect to the firm covalent binds between the thiol groups of the cross-linkers and the gold substrate.

The results revealed that for plasma samples in combination with different concentration of CEA, the response of the immunosensor increased in comparison with the control, proposing that the fabricated immuno-device is desirable for CEA determination in different plasma samples. Thus, the suggested immunosensor can be used as an efficient diagnostic approach for cancer therapy. Generally, the designed immunodevices can introduce a novel technique for simple, rapid, label-free, and costly affordable monitoring of CEA compared to the previous reports. Moreover, the intrinsic rigidity of the polymer may lead to long-term stability, robustness, and re-usability of the synthesized MIP-based biosensor. This method seems to be appropriate for POC usages in clinical context.

3.3.3 | Kinetic studies

Scan rate plays a pivotal role in the electrochemical feature of analytes on the surface of the modified electrode. Thus, the influence of this factor on the electrochemical response of MIP-based gold electrode was evaluated in the presence of 0.1 mM Fe $(CN)_6^{3-/4-}$ containing 0.1 M KCL, (pH = 7.4). The results of the scan rate, recorded between 10 to 100 mV/s, are exhibited in Figure S8A, which reveals that the currents of the oxidation peak raised proportionally through the scan rate representing that the designed system has appropriate ability to shuttling electron. According to Figure S8 (A-F), a linear relationship is revealed between the sweep rate, peak current, and peak oxidation at low sweep rates, representing the catalytic nature of the bio-device. Concerning quantitate factors, three parameters of the number of the transferred electrons (n), the electron transfer coefficient (α), and the coated specific surface area (Γ^*) can be determined by Figure S8E, and Figure S8B, respectively.

The following equation is considered for determining the number of the transferred electrons (n), using Figure S8E.

$$E = \left(\frac{n^2F^2}{4RT}\right) \mathrm{Lnv} + \text{constant},$$

where F is the faraday constant, R is the standard gas constant, and T is the temperature (kelvin). Regarding to this work, the number of the transferred electrons are estimated as 1.05.

The specific facial coating of the modified electrode was calculated by means of the CV method through the following equation:

$$I_p = \left(\frac{F^2n^2}{4RT}\right) \mathrm{vA}\Gamma^*.$$

Γ^*: the surface coating of the redox species; n: the potential sweep rate; A: the surface area of electrode ($A = \pi r^2 = 0.0314\ cm^2$).[44]

In this work, Γ^* is measured around 42×10^{-9} mol cm^{-2}.

It is worth attention that various transport phenomena and the chemical reaction rate depend to a variety of factors such as the flow rate, temperature, the average pore size, the size of particle, and etc. Thus, under certain conditions, the similar reaction can be occurred in the kinetic region, while others can take place in the diffusion region. The adsorption-controlled phenomenon is a process taking place due to the migration of particles or molecules from the bulk phase to the interface. On the other hand, in a diffusion-controlled phenomenon, the molecules are migrated from bulk phase to the subsurface, which then transport from subsurface to interface. Thus, a surface-controlled procedure is explained via the rate of molecule migration from the bulk to the interface, while a diffusion-controlled procedure is characterized by the rate of molecules that diffuse initially through the subsurface and then to the interface. Both phenomena (whether adsorption or diffusion) are scan rate dependent. By plotting a graph log of current vs the log of scan rate, the slope values can be measured between 0.5 and 1, which indicates diffusion-controlled phenomenon for the slope values around 0.5, and adsorption-controlled process for the slope values around 1. According to the results of Figure S8D, the slop of the LnI *vs* LnV linear diagram is measured about 0.4024 which is around 0.5, representing the dominance of the diffusion-controlled phenomenon. Furthermore, According to Figure S8C, and Figure S8B, electron transfer process was controlled by diffusion.

According to the obtained results, it can be concluded that the surface of the electrode has successfully covered by the polymer through an electropolymerization process. Thus, the transmission of the electrons can be improved in the PTB-modified gold electrode.

In order to evaluate the mass transfer mechanism, two methods were suggested. First, the relation between the square root of scan

rate and the peak current was obtained (Figure S8C). Its relevant regression equation is as follows:

$$I\,(\mu A) = 4.5021\,v^{0.5} + 2.8272$$

Applying this approach, the peak current intercept vs the scan rate square root was found to be 3.5443, which demonstrates that the most effective factor to manage mass transfer is diffusion mechanism instead of adsorption, and the bio-device can be used for quantitative analysis. Second, the Napierian logarithm related to scan rate *vs* the Napierian logarithm of peak current was drawn, as illustrating in Figure S8D. The relevant plot slope to the oxidation peak in Figure S8D was found as 0.4024. If the Ln scan rate (V/s) vs the peak current slope (mA) is close to 0.5, then the procedure is diffusion controlled; on the other side, if the rate of slope is close to 1, then the procedure is controlled via adsorption. As, the slope was calculated as 0.4024, it can be resulted that the process of mass transfer is controlled by diffusion, which is in accordance with the recorded results of the previous method. Moreover, the mechanism of mass transfer can further be estimated by the coefficient of the electron transfer (α) of the following Equation[44,45]:

$$Ep = \left(\frac{RT}{2\alpha F}\right)\ln v + \text{constant},$$

E_p: electrode potential, R: standard gas constant (8.314, J K^{-1} mol^{-1}), F: Faraday's constant (96 486, A.s.mol^{-1}), T: temperature in Kelvin scale (298 K), and υ: the potential sweep rate (V/s).

If the rate of α is close to 0.5, the type of the system is diffusion controlled. By means of this equation, the value of α was achieved as 0.018 which also supports that the relevant mass transfer to the system is quasi-reversible and obey from two electron/two proton process. The plot of the aforementioned equation achieved from corresponding peaks potential (V) vs Napierian logarithm of oxidation peak currents (mA) is illustrated at Figure S8E. This diagram reveals the dependency between E_p and the Napierian logarithm of the sweep rate (ln v) of the PTB-coated electrode, its relevant regression equation is as follows:

$$\text{Ln}\,I_p\,(\mu A) = 0.018\,\text{Ln}(v) + 0.208.$$

Although SEM technique can provide information about the structural and topographical features of the prepared electrode surface, there is no imaging technique to evaluate the exact electroactive area, and the electrochemically active/inactive sites on the surface of the electrodes.

Several samples represent a reversible cyclic voltammetric wave that arises from the recovery of all the prototype particles after a reciprocating sweep.

The variances between the obtained potential peaks (E, p), called ΔE p, are shown as follows which has gained a particular interest:

$$\Delta Ep = E_{pc} - E_{pa.}$$

This variance is chiefly depended to the sample diffusion rate. Also, the waveform is under influence of the electron transfer velocity, which can be considered as the activation hindrance for electron transfer.

By considering the flow, the ideal model of the reversible pairs follows the relation of $\frac{I_{pa}}{I_{pc}} = 1$. For the semi-reversible pairs, I_{pa} is close to I_{pc}, but not equal. According to Figure S8F, since the slope of the curve is close to zero (–0.001), not exactly zero, the relation of $\frac{I_{pa}}{I_{pc}}$ is close to 1, not exactly 1, which indicated that the system follows a semi-reversible process. The data in Figure S8 also indicate that the oxidative (i_p ox) peak to reductive (i_p red) peak currents ratio (i_p ox/i_p red) kept approximately constant by raising the scan rate, while ΔE_{pp} (the peak-to-peak separation of the anodic (E_p ox) to cathodic (E_p red)) raised with growing scan rate.

In this work, according to Figure S8D, ΔE_p (the peak-to-peak separation) was 0.1 V and the I_{ox}/ I_{red} (current peak ratio) for the MIP-modified gold electrode was approximately a unit, demonstrating that the electrochemical procedure of the prepared electrode is quasi-reversible; its relevant regression equation is as follows:

$$I\,(\mu A) = -0.0011\,v + 0.6169.$$

This indication reveals that the great surface area to volume ratio achieved from electrodeposition of TB on the premodified gold electrode improved the electron transfer within the system. The impact of scan rate in the CV curves of the PTB-coated gold electrode was examined in 0.1 M $[Fe\,(CN)_6]^{3-/4-}$ solution containing KCl. According to Figure S8A, a pair of redox peaks obtained at different scan rates and the current of the redox peak changed linearly by increasing the scan rate within the range of 10 to 100 mV.S^{-1}. The linear diagram in the Figure S8B also reveals the linear relationship that occurred between the scan rate and peak current.

3.4 | Stability Study of CEA-imprinted polymer

Stability is one of the most important factors of a biosensor that tightly depends on its application. The stability and repeatability of the MIP-based biosensors are considered as the most pivotal features for their long-term application in sensing assays. In this work, the stability of the MIP-based biosensor was evaluated through CV analytical tests in $Fe\,(CN)_6^{3-/4-}$ (0.1 M) comprising 0.1 M KCl. The signal alternations of the relevant peak currents to the MIP-based biosensor were recorded after 24 hours storage of the electrodes at 4°C (Figure 6). The results showed a slight decrement in the peak currents of the incubated electrode after 24 hours, declaring reasonable stability of the synthesized bioassay.

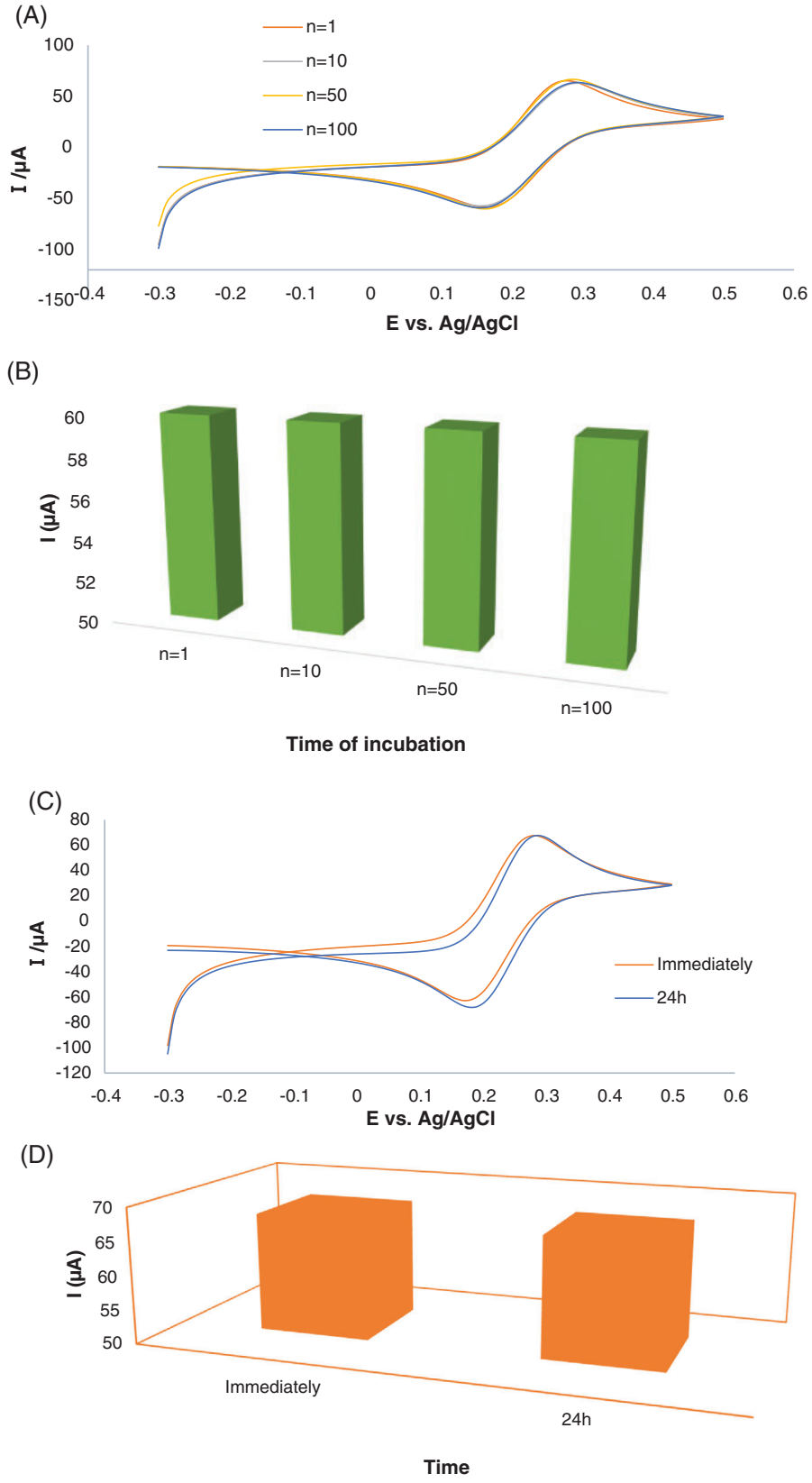

FIGURE 6 A, E, Cyclic voltammetry of biosensor in the potential range of −0.3 to 0.5 and sweep rate of 40 mV/s in 1 mM of Fe $(CN)_6^{3-/4-}$ In different cycle numbers and different incubation time at −4°C. B, D. Histogram of peak current vs number of cycles and time of storage, respectively

4 | CONCLUSIONS

In this study, sensitive detection of carcinoembryonic antigen (CEA) was evaluated by using the electrically conductive poly (Toluidine Blue (PTB)) as receptor, accompanied by the molecular imprinting methods and electrochemical approaches. The electropolymerization of the CEA-imprinted PTB on the pretreated gold electrode surface (using cysteamine and glutaraldehyde as the cross-linkers) led to improve

the stability of the system against the degrading factors of the molecular-imprinted polymer (MIP). Moreover, electrochemical methods were performed to evaluate the potential of the MIP-based immunosensor toward the protein detection. In comparison with the nonimprinted polymer (NIP) bio-device, the MIP-based system had considerably higher binding affinity. This superiority of the MIP-based systems over the NIP-based ones caused to make it more efficient in fabricating imprinted materials that are particularly favorable for CEA biomarker monitoring. Various concentrations of CEA (from 0.005 to 75 μg/L) were considered for entrapping through the PTB matrix coated on the gold electrode, the results revealed an increase in the 0.1 mM of $Fe(CN)_6^{3-/4-}$ redox peak current. It was further revealed that the prepared immunosensor possessed a broad linear range from 0.005 to 75 μg/L and LLOQ of 0.005 μg/L with a great selectivity, affinity, and acceptable stability, representing the successful monitoring of the CEA in clinical samples. The designed immunosensor is also likely to offer a novel strategy for rapid, simple, sensitive, and costly affordable evaluating of 0.005 μg/L of CEA. Furthermore, the technique appears to be suitable for point-of-care (POC) applications in biomedical and clinical analysis. Interestingly, other types of template molecules can be applied in our proposed MIP-based system for designing new immunosensors to monitor other target biomolecules.

ACKNOWLEDGEMENT

The authors thank Tabriz University of Medical Sciences for instrumental supporting of this research.

CONFLICT OF INTEREST

There is no conflict of interest.

DATA AVAILABILITY STATEMENT

The data that support the findings of this study are available from the corresponding author upon reasonable request.

ORCID

Parinaz Abdollahiyan https://orcid.org/0000-0002-9599-0558
Mohammad Hasanzadeh https://orcid.org/0000-0003-4918-1239

REFERENCES

1. Hasanzadeh M, Shadjou N, Lin Y, de la Guardia Guardia M, et al. *Nanomaterials for use in immunosensing of carcinoembryonic antigen (CEA): Recent advances*. Trends Anal Chem. 2017;86:185-205.
2. Kim S, Kim TG, Lee SH, Bang A, Moon SW, Song J, Shin JH, Yu JS, Choi S. *Label-free surface-enhanced raman spectroscopy biosensor for on-site breast cancer detection using human tears*. ACS Appl Mater Interfaces. 2020;12(7):7897-7904.
3. Hasanzadeh M, Shadjou N. *Early stage screening of breast cancer using electrochemical biomarker detection*. Trends Anal Chem. 2017;91:67-76.
4. Xu Z, Han R, Liu N, Gao F, Luo X. *Electrochemical biosensors for the detection of carcinoembryonic antigen with low fouling and high sensitivity based on copolymerized polydopamine and zwitterionic polymer*. Sens Actuators B. 2020;319:128253.
5. Jandas PJ, Luo J, Quan A, et al. *Highly selective and label-free love-mode surface acoustic wave biosensor for carcinoembryonic antigen detection using a self-assembled monolayer bioreceptor*. Appl Surf Sci. 2020;518:146061.
6. Wang L. *Screening and biosensor-based approaches for lung cancer detection*. Sensors (Basel). 2017;17(10):2420.
7. Zhang X, Yu Y, Shen J, Qi W, Wang H. *Design of organic/inorganic nanocomposites for ultrasensitive electrochemical detection of a cancer biomarker protein*. Talanta. 2020;212:120794.
8. Abbasy L, Mohammadzadeh A, Hasanzadeh M, Razmi N. *Development of a reliable bioanalytical method based on prostate specific antigen trapping on the cavity of molecular imprinted polymer towards sensing of PSA using binding affinity of PSA-MIP receptor: a novel biosensor*. J Pharm Biomed Anal. 2020;188:113447.
9. Pirzada M, Sehit E, Altintas Z. *Cancer biomarker detection in human serum samples using nanoparticle decorated epitope-mediated hybrid MIP*. Biosens Bioelectron. 2020;166:112464.
10. Curk T, Dobnikar J, Frenkel D. *Rational design of molecularly imprinted polymers*. Soft Matter. 2016;12(1):35-44.
11. Saeki T, Takano E, Sunayama H, et al. *Signalling molecular recognition nanocavities with multiple functional groups prepared by molecular imprinting and sequential post-imprinting modifications for prostate cancer biomarker glycoprotein detection*. J Mater Chem B. 2020;8(35):7987-7993.
12. Hasanzadeh M, Shadjou N, de la Guardia M. *Cytosensing of cancer cells using antibody-based molecular imprinting: a short-review*. TrAC Trends Anal Chem. 2018;99:129-134.
13. Ma Y, Yin Y, Ni L, et al. *Thermo-responsive imprinted hydrogel with switchable sialic acid recognition for selective cancer cell isolation from blood*. Bioactive Materials. 2021;6(5):1308-1317.
14. Kweinor Tetteh E, Rathilal S, Amankwa Opoku M, Amoah ID, Chollom MN. *Molecular imprinting technology: a new approach for antibacterial materials*. In: Inamuddin MIA, Prasad R, eds. *Advanced Antimicrobial Materials and Applications*. Singapore: Springer Singapore; 2021:393-421.
15. Zaidi SA. *Molecular imprinting: a useful approach for drug delivery*. Materials Science for Energy Technologies. 2020;3:72-77.
16. Xu J, Miao H, Wang J, Pan G. *Molecularly imprinted synthetic antibodies: from chemical design to biomedical applications*. Small. 2020;16(27):1906644.
17. Ma X, Tu X, Gao F, et al. *Hierarchical porous MXene/amino carbon nanotubes-based molecular imprinting sensor for highly sensitive and selective sensing of fisetin*. Sens Actuators B. 2020;309:127815.
18. Sardaremelli S, Hasanzadeh M, Razmi H. *Chemical binding of horseradish peroxidase enzyme with poly beta-cyclodextrin and its application as molecularly imprinted polymer for the monitoring of H2O2 in human plasma samples*. J Mol Recog. 2021;34(5):e2884. https://onlinelibrary.wiley.com/doi/abs/10.1002/jmr.2884.
19. Drzazgowska J, Schmid B, Süssmuth RD, Altintas Z. *Self-assembled monolayer epitope bridges for molecular imprinting and cancer biomarker sensing*. Anal Chem. 2020;92(7):4798-4806.
20. Moreira Gonçalves L. *Electropolymerized molecularly imprinted polymers: perceptions based on recent literature for soon-to-be world-class scientists*. Current Opinion in Electrochemistry. 2021;25:100640.
21. Khanmohammadi A, Aghaie A, Vahedi E, et al. *Electrochemical biosensors for the detection of lung cancer biomarkers: a review*. Talanta. 2020;206:120251.
22. Farshchi F, Hasanzadeh M. *Biomedicine & Pharmacotherapy*. Biomed Pharmacother. 2021;134:111153.
23. Saadati A, Hassanpour S, Hasanzadeh M, et al. *A novel electrochemical epinine sensor using amplified CuO nanoparticles and a n-hexyl-3-methylimidazolium hexafluorophosphate electrode*. Heliyon. 2020;6(12):e05779.
24. Farshchi F, Hasanzadeh M. *Nanomaterial based aptasensing of prostate specific antigen (PSA): Recent progress and challenges in efficient diagnosis of prostate cancer using biomedicine*. Biomed Pharmacother. 2020;132:110878.
25. Jafari M, Hasanzadeh M. *Non-invasive bioassay of Cytokeratin Fragment 21.1 (Cyfra 21.1) protein in human saliva samples using immunoreaction method: An efficient platform for early-stage diagnosis of oral*

cancer based on biomedicine. Biomed Pharmacother. 2020;131:110671.
26. Wang J, Hui N. *Zwitterionic poly(carboxybetaine) functionalized conducting polymer polyaniline nanowires for the electrochemical detection of carcinoembryonic antigen in undiluted blood serum*. Bioelectrochemistry. 2019;125:90-96.
27. Wang Y, Zhao G, Zhang Y, et al. *Sandwich-type electrochemical immunosensor for CEA detection based on Ag/MoS2@Fe_3O_4 and an analogous ELISA method with total internal reflection microscopy*. Sens Actuators B. 2018;266:561-569.
28. Mazloum-Ardakani M, Barazesh B, Moshtaghioun SM. *An aptasensor based on electrosynthesized conducting polymers, Cu_2O carbon dots and biosynthesized gold nanoparticles, for monitoring carcinoembryonic antigen*. J Nanostruct. 2019;9:659-668.
29. Feng D, Lu X, Dong X, Ling Y, Zhang Y. *Label-free electrochemical immunosensor for the carcinoembryonic antigen using a glassy carbon electrode modified with electrodeposited Prussian blue, a graphene and carbon nanotube assembly and an antibody immobilized on gold nanoparticles*. Microchimica Acta. 2013;180(9):767-774.
30. Pavithra M, Muruganand S, Parthiban C. *Development of a simple Isatin-based electrochemical Immunosensor on a screen-printed gold electrode for highly sensitive detection of Carcinoembryonic antigen*. ChemistrySelect. 2017;2(24):7239-7245.
31. Li Y, Yang WK, Fan MQ, Liu A. *A sensitive label-free amperometric CEA immunosensor based on graphene-nafion nanocomposite film as an enhanced sensing platform*. Anal Sci. 2011;27(7):727.
32. Wang Z, Tian X, Sun D, et al. *A new Bi_2MoO_6 nano-tremella-based electrochemical immunosensor for the sensitive detection of a carcinoembryonic antigen*. RSC Adv. 2020;10(27):15870-15880.
33. Lin X, Li S, Zhang B, Yang H, Zhang K, Huang H. *An enzyme-free fluorescent biosensor for highly sensitive detection of carcinoembryonic antigen based on aptamer-induced entropy-driven circuit*. Anal Methods. 2020;12(45):5496-5502.
34. Zhao L, Cheng M, Liu G, et al. *A fluorescent biosensor based on molybdenum disulfide nanosheets and protein aptamer for sensitive detection of carcinoembryonic antigen*. Sens Actuators B. 2018;273:185-190.
35. Wang K, He M-Q, Zhai F-H, He R-H, Yu Y-L. *A label-free and enzyme-free ratiometric fluorescence biosensor for sensitive detection of carcinoembryonic antigen based on target-aptamer complex recycling amplification*. Sens Actuators B. 2017;253:893-899.
36. Li J, Zhao L, Wang W, et al. *Polymer-functionalized carbon nanotubes prepared via ring-opening polymerization for electrochemical detection of carcinoembryonic antigen*. Sens Actuators B. 2021;328:129031.
37. Crapnell RD, Dempsey-Hibbert NC, Peeters M, Tridente A, Banks CE. *Molecularly imprinted polymer based electrochemical biosensors: overcoming the challenges of detecting vital biomarkers and speeding up diagnosis*. Talanta Open. 2020;2:100018.
38. Li R, Feng Y, Pan G, Liu L. *Advances in molecularly imprinting Technology for Bioanalytical Applications*. Sensors (Basel). 2019;19(1):177.
39. Cui F, Zhou Z, Zhou HS. *Molecularly imprinted polymers and surface imprinted polymers based electrochemical biosensor for infectious diseases*. Sensors. 2020;20(4):996.
40. Ertürk G, Mattiasson B. *Molecular imprinting techniques used for the preparation of biosensors*. Sensors. 2017;17(2):288.
41. Santos GS, Caldas RGSC, Melo FL, et al. *Label-free nanostructured biosensor for* Schistosoma mansoni *detection in complex biological fluids*. Talanta. 2019;204:395-401.
42. Aggas JR, Guiseppi-Elie A. *2.5.13 - responsive polymers in the fabrication of enzyme-based biosensors*. In: Wagner WR, Sakiyama-Elbert SE, Zhang G, Yaszemski MJ, eds. *Biomaterials Science*. 4th ed. Netherlands: Academic Press; 2020:1267-1286.
43. Ribeiro J, Pereira C, Silva AF, Sales MG. *Disposable electrochemical detection of breast cancer tumour marker CA 15-3 using poly(toluidine blue) as imprinted polymer receptor*. Biosens Bioelectron. 2018;109:246-254.
44. García-Miranda Ferrari A, Foster CW, Kelly PJ, Brownson DAC, Banks CE. *Determination of the electrochemical area of screen-printed electrochemical sensing platforms*. Biosensors. 2018;8(2):53.
45. Thomas D, Rasheed Z, Jagan JS, Kumar KG. *Study of kinetic parameters and development of a voltammetric sensor for the determination of butylated hydroxyanisole (BHA) in oil samples*. J Food Sci Technol. 2015;52(10):6719-6726.

SUPPORTING INFORMATION

Additional supporting information may be found online in the Supporting Information section at the end of this article.

How to cite this article: Abdollahiyan P, Mohammadzadeh A, Hasanzadeh M. Chemical binding of molecular-imprinted polymer to biotinilated antibody: Utilization of molecular imprinting polymer as intelligent synthetic biomaterials toward recognition of carcinoma embryonic antigen in human plasma sample. *J Mol Recognit*. 2021;e2897. https://doi.org/10.1002/jmr.2897